A&A 446, 1185–1190 (2006)
DOI: 10.1051/0004-6361:20053813

Astronomy & Astrophysics

Electron collisions with Fe-peak elements: Fe IV

I. Forbidden transitions: $3d^5 - 3d^4 4s$ and $3d^5 - 3d^4 4p$ manifolds⋆

B. M. McLaughlin[1], A. Hibbert[1], M. P. Scott[1], C. J. Noble[2], V. M. Burke[2], and P. G. Burke[1]

[1] School of Mathematics and Physics, Queen's University of Belfast, Belfast BT7 1NN, UK
e-mail: b.mclaughlin@qub.ac.uk
[2] Computational Science and Engineering Department, CCLRC Daresbury Laboratory, Keckwick Lane, Daresbury, Warrington WA4 4AD, UK

Received 11 July 2005 / Accepted 26 September 2005

ABSTRACT

Electron-impact excitation collision strengths of the Fe-peak element Fe IV are calculated in the close-coupling approximation using the parallel *R*-matrix program PRMAT. One hundred and eight *LS* – coupled states arising from the $3d^5$, $3d^4 4s$ and $3d^4 4p$ configurations of Fe IV, are retained in the present calculations. Accurate multi-configuration target wavefunctions are employed with the aid of $3p^2 \rightarrow 3d^2$ electron promotions and a $\overline{4d}$ correlation orbital. The effective collision strengths required in the analysis of astrophysically important lines in the Fe IV spectra, are obtained by averaging the electron collision strengths for a wide range of incident electron energies, over a Maxwellian distribution of velocities. Results are tabulated for forbidden transitions between the $3d^5$, $3d^4 4s$ and the $3d^4 4p$ manifolds for electron temperatures (T_e in degrees Kelvin) in the range $3.3 \leq \mathrm{Log}\, T_e \leq 6.0$ that are applicable to many laboratory and astrophysical plasmas. The present results provide new results for forbidden lines in the Fe IV spectrum studied here.

Key words. atomic data – atomic processes

1. Introduction

For electron impact excitation of V-like ions (Mn III, Fe IV, Co V and Ni VI), new astronomical observations are revealing the presence of trace metals in many types of astronomical objects. High-dispersion IUE observations of the brightest of the hot stars showed absorption features from photospheric Fe and Ni (Holberg et al. 1994); identifications included V-like Fe and Ni ions; i.e. Fe IV and Ni VI lines. From these observations Ni became the second iron group element to be positively identified in the photosphere of the hot DA white dwarfs. Adelman and co-workers (Adelman et al. 1994) have analysed the abundances of elements such as Cr, Mn, Fe, Co and Ni in early type stars from IUE high-dispersion spectrograms. Ruiz-Lapuente et al. (1995) reviewed observations of Type Ia supernovae at late phases, which range from the UV to the infrared region. Calculations of spectra of different Type Ia models have shown the need for further computations of collision strengths for forbidden transitions of Fe I-IV (Ruiz-Lapuente et al. 1995). In supernovae 1992A among the identified forbidden transitions giving rise to UV emission lines in *Hubble Space Telescope* (HST) spectra are the following V-like ions Fe IV (^{6}S–^{4}D), Fe IV (^{6}S–^{4}P) and Mn III (^{6}S–^{4}D). In the Orion nebulae, the first detection of an Fe IV line in a H II region has been made using the Goddard High-Resolution Spectrograph on the *Hubble Space Telescope*, where the flux of the [Fe IV]($3d^5\ ^4P_{5/2} \rightarrow 3d^5\ ^6S_{5/2}$), $\lambda_{\mathrm{vac}} = 2836.56$ Å line has been measured (Rubin et al. 1997). Fe IV lines have also been detected in symbiotic nova such as RR TELESCOPII (RR Tel) based on International Ultraviolet Explorer (IUE) observations (Penston et al. 1983) and more recently by the telescope of the Cerro Tololo Inter-American Observatory (McKenna et al. 1997). A recent reappraisal of the chemical composition of the Orion nebulae (Estan et al. 2004) based on Very Large Telescope (VLT) UVES echelle spectromphotometery illustrated vividly the need to have accurate atomic data on several of the Fe-peak elements, namely low ionization stages of Fe, Ni and Co. Furthermore, accurate electron impact excitation rates for low ionization stages of Fe-ions (Fe II–Fe V) are required for non-LTE calculations in hot stars atmospheres (Becker & Butler 1995) and winds. The present work on the Fe-peak element Fe IV attempts to provide accurate atomic data suitable for relevant applications.

2. Theory

We solved the multi-state, many-bodied Schrödinger equation for this complex ion within the confines of the *R*-matrix close-coupling method (Burke & Robb 1975) using the

⋆ Tables 2–17 are only available in electronic form at the CDS via anonymous ftp to cdsarc.u-strasbg.fr (130.79.128.5) or via http://cdsweb.u-strasbg.fr/cgi-bin/qcat?J/A+A/446/1185

parallel suite of codes PRMAT (Sunderland et al. 1999; Sunderland et al. 2002; Noble 2004; Burke et al. 2004; and Noble et al. 2005) to calculate the $\mathcal{K}$ matrices and the cross sections $\sigma(i \rightarrow j)$ for a specific orbital angular momentum L, spin angular momentum S and parity Π. We have calculated the total collision strength Ω where

$$\Omega(i, j) = \sum_{LS\Pi} \Omega^{LS\Pi}(i, j) \quad (1)$$

is related to the total cross section, $\sigma(i, j)$ for the case of transitions between $LS\pi$ levels by

$$\Omega(i, j) = (2L + 1)(2S + 1)k_i^2\sigma(i, j). \quad (2)$$

The total cross sections for the excitation of an ion from state L_iS_i to excited state L_jS_j is obtained from,

$$\sigma\left(L_iS_i \rightarrow L_jS_j\right) = \frac{\pi}{2k_i^2} \sum_{LS\ell_i\ell_j\Pi} \frac{(2L + 1)(2S + 1)}{(2L_i + 1)(2S_i + 1)} \left|\mathcal{S}_{ij} - \delta_{ij}\right|^2 \quad (3)$$

where the $\mathcal{S}$ -matrix is related to the $\mathcal{K}$ matrix by the relation

$$\mathcal{S} = \frac{\mathcal{I} + i\mathcal{K}}{\mathcal{I} - i\mathcal{K}}. \quad (4)$$

While the collision strength defined above is often useful in its own right, more frequently, in application, it is assumed that the scattering electrons have a Maxwellian velocity distribution. Effective collision strengths (Υ) and rate coefficients (q) are therefore the desired quantities (McLaughlin et al. 2005a). The effective collision strength (Υ), for a transition from state i to state j is then obtained by averaging the collision strength over a Maxwellian velocity distribution and is defined as follows:

$$\Upsilon(i, j) = \int_o^\infty \Omega(i, j) \exp(-\epsilon_i/k_B\mathrm{T_e})\, \mathrm{d}(\epsilon_i/k_B\mathrm{T_e}). \quad (5)$$

Here ϵ_i is the final kinetic energy of the scattered electron when the target ion is in state i, k_B is Boltzmann's constant and T_e is the electron temperature in degrees Kelvin.

For many applications the rate coefficient, in $\mathrm{cm^3\ s^{-1}}$, is required as a function of electron temperature. The rate coefficient can be determined for transition $j \rightarrow i$ corresponding to de-excitation (when $E_j > E_i$) from the effective collision strength via the relationship (Eissner et al. 1969),

$$q(j, i) = \frac{8.63 \times 10^{-6}}{g_i\ \sqrt{T_\mathrm{e}}}\ \Upsilon(j, i) \quad (6)$$

where $g_i = (2L_i + 1)(2S_i + 1)$ is the statistical weight of level i and the effective collision strength $\Upsilon(j, i)$ is given by:

$$\Upsilon(j, i) = \int_o^\infty \Omega(i, j) \exp(-\epsilon_j/k_B\mathrm{T_e})\, \mathrm{d}(\epsilon_j/k_\mathrm{B}T_\mathrm{e}). \quad (7)$$

For excitation, the rate coefficient may be obtained via the detailed balance expression

$$q(i, j) = \frac{(2L_j + 1)(2S_j + 1)}{(2L_i + 1)(2S_i + 1)} q(j, i) \exp(\Delta E_{ij}/k_\mathrm{B}T_\mathrm{e}). \quad (8)$$

Here $\Delta E_{ij} = E_i - E_j$ is the internal energy difference between states i and j.

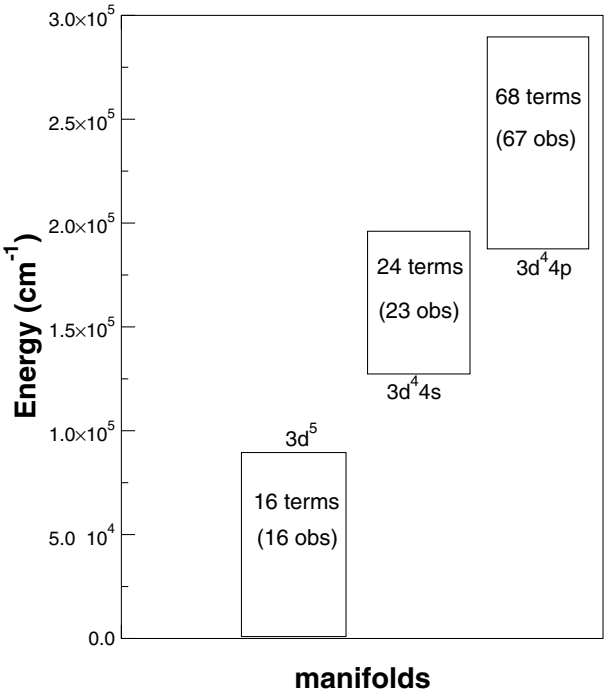

Fig. 1. Observed Fe IV levels in $\mathrm{cm^{-1}}$ associated with the three configurations $3d^5$, $3d^4 4s$ and $3d^4 4p$ from the NIST tables. All of the levels of the $3d^5$ manifold are observed whereas only 23 of the 24 levels for $3d^4 4s$ and 67 of the 68 levels of the $3d^4 4p$ manifolds are observed.

3. Details of calculations

As an indication of the complexity of the problem for electron-impact collisions with Fe IV ions we show in Fig. 1 the number of LS – coupled target states which arise from the three configurations; $3d^5$, $3d^4 4s$ and $3d^4 4p$. We note that the sheer size of the problem doubles (both in the number of states and coupled channels) by including those states arising from the inclusion of the $3d^4 4d$ configuration, none of which have been observed (cf. NIST tables, `http://physics.nist.gov/cgi-bin/AtData/main_asd`, Sugar & Corliss 1985). These states were omitted as structure calculations indicated they lay sufficiently higher than the rest. In our work we retained in the R-matrix expansion all 108 LS-coupled states which arise from the $3d^5$, $3d^4 4s$ and $3d^4 4p$ configurations of Fe IV. Our recent investigation on this complex ion dealt with transitions within the $3d^5$ manifold (McLaughlin et al. 2005b). In that work is was seen that with the inclusion of suitably correlated target and scattering wavefunctions the effective collision strengths were enhanced by a factor of two, particularly at temperatures below 100 000 Kelvin. The main thing to note from our recent work on Fe IV was that it was essential to include the two electron promotions $3p^2 \rightarrow 3d^2$ in the target wavefunctions in order to have an adequate representation of the target energies (Hibbert et al. 2004; Quintet & Hansen 1995). It should be pointed out that the number of coupled scattering channels and target states would vastly

increase if fine structure effects are included in the calculation as does the computational complexity. Prior to our investigation on electron impact excitation of Fe IV (McLaughlin et al. 2004, 2005b), previous work (Sawey & Berrington 1992; Berrington & Pelan 1995a,b; Zhang & Pradhan 1997), included only a limited number (5 and 49 states respectively) of the 108 $LS\pi$ states which may arise from the three Fe IV configurations $3d^5$, $3d^4 4s$, $3d^4 4p$ in scattering calculations. We note that in our work we include all of the terms which can arise from each of the configuration which is necessary to obtain reliable results.

In the current study, results are presented for forbidden transitions between the manifolds $3d^5$–$3d^4 4s$ and $3d^5$–$3d^4 4p$. As in our recent work (McLaughlin et al. 2005b) on this complex ion, the 108 states of Fe IV are represented by multi-configuration interaction wavefunctions in the corresponding close-coupling calculations. Hartree-Fock orbitals of the $1s^2 2s^2 2p^6 3s^2 3p^6 3d^5\ ^6S$ ground state configuration augmented with two spectroscopic orbitals namely, the 4s and 4p and $\overline{4d}$ correlation orbital are employed. The 1s, 2s, 2p, 3s, 3p and 3d orbitals used were taken from the the work of Clementi & Roetti (1974). The additional orbitals used are determined from the structure codes CIV3 (Hibbert 1975). Using a seven configuration model; $3d^5$, $3d^4 4s$, $3d^4 4p$, $3d^4\overline{4d}$, $3p^4 3d^7$, $3p^4 3d^6 4s$ and $3p^4 3d^6 4p$ we found that this gave a compact and adequate CI representation for all of the 108 levels of Fe IV arising from the $3d^5$, $3d^4 4s$ and $3d^4 4p$ configurations (see Table 1), with term energies differing from experiment by approximately a few percent. These compact CI target wavefunctions for Fe IV were then used in our scattering calculations. All the cross section and effective collision strengths were obtained with this seven configuration model; $3d^5$, $3d^4 4s$, $3d^4 4p$,$3d^4\overline{4d}$, $3p^4 3d^7$, $3p^4 3d^6 4s$ and $3p^4 3d^6 4p$ as outlined in our recent work. The relevant collision calculations were performed with the PRMAT suite of codes (Sunderland et al. 1999, 2002; Noble 2004; Burke et al. 2004; and Noble et al. 2005). Cross section calculations for total scattering angular momentum $L \leq 12$ for all spin symmetries $2S + 1$ equal to 1, 3, 5 and 7, i.e. for singlets, triplets, quintets and septets were then carried out for both odd and even parities of the collision system. Further details of the collision calculations can been found in our recent work (McLaughlin et al. 2005b) on this system and will not be expanded upon here.

Table 1 gives the theoretical energies of the 108 states included in the present approximation (7 configuration model) and includes the adjustment required to the theoretical values so as to reproduce the available observed values (NIST tables, `http://physics.nist.gov/cgi-bin/AtData/main_asd`, Sugar & Corliss 1985). It should be pointed out that some of the 108 states of Fe IV included in the present approximation have not been observed but are present due to LS-coupling and they will play an important role as intermediate states in the calculation. Hence, where no observed values are available for a specific term we have made a similar adjustment to its theoretical value as that made to the ground-state term. The same labelling of the states is used to identify transitions from state i to state j for the effective collision strengths tabulated in Tables 2–17.

Table 1. Term energies (Rydbergs) for the 108-states of Fe IV relative to the $3d^5\ ^6S$ state. Theoretical energies (7 configuration model) are compared with observed values and the theoretical adjustment to reproduce experimental values.

Label	Term	Calculated	Observed[†]	Adjustment
1	$3d^5\ ^6S$	0.000000	0.000000	0.066360
2	$3d^5\ ^4G$	0.340789	0.294169	0.019740
3	$3d^5\ ^4P$	0.346937	0.321730	0.041153
4	$3d^5\ ^4D$	0.401853	0.354206	0.018713
5	$3d^5\ ^2I$	0.502193	0.429070	–0.006763
6	$3d^5\ ^2D3$	0.503829	0.453314	0.015845
7	$3d^5\ ^2F2$	0.515790	0.471355	0.021925
8	$3d^5\ ^4F$	0.529654	0.480415	0.017121
9	$3d^5\ ^2H$	0.572988	0.512384	0.005755
10	$3d^5\ ^2G2$	0.598621	0.524725	–0.007535
11	$3d^5\ ^2F1$	0.633741	0.557808	–0.009572
12	$3d^5\ ^2S$	0.686992	0.607998	–0.012634
13	$3d^5\ ^2D2$	0.747154	0.675417	–0.005377
14	$3d^5\ ^2G$	0.844320	0.755403	–0.022557
15	$3d^5\ ^2P$	1.015938	0.912366	–0.037212
16	$3d^5\ ^2D1$	1.079566	0.986433	–0.026773
17	$3d^4(^5D)4s\ ^6D$	1.199945	1.170798	0.037213
18	$3d^4(^5D)4s\ ^4D$	1.299893	1.261185	0.027653
19	$3d^4(^3H)4s\ ^4H$	1.480181	1.407728	–0.006093
20	$3d^4(^3P2)4s\ ^4P$	1.457862	1.412214	0.020712
21	$3d^4(^3F2)4s\ ^4F$	1.485450	1.422742	0.003652
22	$3d^4(^3G)4s\ ^4G$	1.529671	1.450156	–0.013155
23	$3d^4(^3H)4s\ ^2H$	1.541618	1.463187	–0.012071
24	$3d^4(^3P2)4s\ ^2P$	1.519275	1.467622	0.014707
25	$3d^4(^3F2)4s\ ^2F$	1.545497	1.476999	–0.002137
26	$3d^4(^3G)4s\ ^2G$	1.591180	1.505376	–0.019443
27	$3d^4(^3D)4s\ ^4D$	1.600647	1.509077	–0.025210
28	$3d^4(^1G2)4s\ ^2G$	1.611736	1.528645	–0.016731
29	$3d^4(^1I)4s\ ^2I$	1.631546	1.535893	–0.029294
30	$3d^4(^1S2)4s\ ^2S$	1.641660	1.555800	–0.019499
31	$3d^4(^3D)4s\ ^2D$	1.658916	1.561890	–0.030666
32	$3d^4(^1D2)4s\ ^2D$	1.687886	1.613217	–0.008308
33	$3d^4(^1F)4s\ ^2F$	1.779029	1.669097	–0.043572
34	$3d^4(^5D)4p\ ^6F^o$	1.725687	1.724548	0.065221
35	$3d^4(^3P1)4p\ ^6P^o$	1.735382	1.732117	0.063095
36	$3d^4(^3F1)4s\ ^4F$	1.843385	1.734926	–0.042099
37	$3d^4(^3P1)4s\ ^4P$	1.843199	1.735790	–0.041049
38	$3d^4(^5D)4p\ ^4P^o$	1.769718	1.754275	0.050916
39	$3d^4(^5D)4p\ ^6D^o$	1.771263	1.761745	0.056842
40	$3d^4(^3F1)4s\ ^2F$	1.901522	1.787627	–0.047534
41	$3d^4(^3P1)4s\ ^2P$	1.899555	1.787916	–0.045278
42	$3d^4(^5D)4p\ ^4F^o$	1.812519	1.791166	0.045006
43	$3d^4(^1G1)4s\ ^2G$	1.956409	1.833406	–0.056643
44	$3d^4(^5D)4p\ ^4D^o$	1.881007	1.843955	0.029308
45	$3d^4(^3H)4p\ ^4H^o$	1.983802	1.938031	0.020589
46	$3d^4(^3P2)4p\ ^4D^o$	1.974759	1.953333	0.044934
47	$3d^4(^3F2)4p\ ^4G^o$	2.003817	1.963041	0.025585
48	$3d^4(^3H)4p\ ^4I^o$	2.016847	1.969818	0.019331
49	$3d^4(^3P2)4p\ ^4P^o$	2.019941	1.970957	0.017375
50	$3d^4[x]4p\ ^4P^o$	2.011385	1.980479	0.035454
51	$3d^4(^3P2)4p\ ^2S^o$	2.006379	1.982986	0.042967
52	$3d^4(^3H)4p\ ^4G^o$	2.038614	1.988392	0.016138
53	$3d^4(^3F2)4p\ ^4F^o$	2.034066	1.989449	0.021744

Table 1. continued.

Label	Term	Calculated	Observed†	Adjustment
54	$3d^4$[y]4p $^4S^o$	2.027023	1.992155	0.031492
55	$3d^4(^3F2)4p\ ^2D^o$	2.035478	1.995303	0.026185
56	$3d^4(^3H)4p\ ^2I^o$	2.060416	2.001191	0.007136
57	$3d^4(^3F2)4p\ ^4D^o$	2.047130	2.002314	0.021544
58	$3d^4(^1S)4p\ ^2P^o$	2.034663	2.004952	0.036650
59	$3d^4(^3G)4p\ ^2F^o$	2.064056	2.008937	0.011241
60	$3d^4(^3H)4p\ ^2H^o$	2.075444	2.012468	0.003383
61	$3d^4(^3G)4p\ ^4F^o$	2.075566	2.016490	0.007284
62	$3d^4(^3G)4p\ ^4H^o$	2.074650	2.018506	0.010215
63	$3d^4(^3P2)4p\ ^2D^o$	2.065025	2.027897	0.029232
64	$3d^4(^1D1)4s\ ^2D$	2.192750	2.030712	–0.095679
65	$3d^4(^3F2)4p\ ^2G^o$	2.095336	2.036926	0.007950
66	$3d^4(^3G)4p\ ^2H^o$	2.105833	2.037948	–0.001526
67	$3d^4(^3F2)4p\ ^2F^o$	2.099502	2.039441	0.006299
68	$3d^4(^3G)4p\ ^4G^o$	2.105367	2.045878	0.006871
69	$3d^4(^3D)4p\ ^4D^o$	2.141671	2.069141	–0.006170
70	$3d^4(^3G)4p\ ^2G^o$	2.145586	2.074366	–0.004859
71	$3d^4(^3D)4p\ ^4P^o$	2.147618	2.080685	–0.000574
72	$3d^4(^1I)4p\ ^2I^o$	2.154102	2.080015	–0.007727
73	$3d^4(^1G2)4p\ ^2F^o$	2.146941	2.083144	0.002563
74	$3d^4(^1G2)4p\ ^2H^o$	2.152353	2.087470	0.001477
75	$3d^4(^3D)4p\ ^4F^o$	2.159976	2.089103	–0.004513
76	$3d^4(^1I)4p\ ^2K^o$	2.166234	2.094619	–0.005256
77	$3d^4(^1S2)4p\ ^2P^o$	2.156113	2.115718	0.025965
78	$3d^4(^1G2)4p\ ^2G^o$	2.181634	2.111013	–0.004262
79	$3d^4(^3D)4p\ ^2P^o$	2.202241	2.104372	–0.031509
80	$3d^4(^1I)4p\ ^2H^o$	2.210925	2.127929	–0.016636
81	$3d^4(^3D)4p\ ^2F^o$	2.214962	2.131639	–0.016963
82	$3d^4(^3D)4p\ ^2D^o$	2.205556	2.138532	–0.000664
83	$3d^4(^1D2)4p\ ^2D^o$	2.238688	2.160953	–0.011375
84	$3d^4(^1D2)4p\ ^2F^o$	2.239250	2.176396	0.003506
85	$3d^4(^1D2)4p\ ^2P^o$	2.280974	2.207627	–0.006987
86	$3d^4(^1F)4p\ ^2F^o$	2.296282	2.212693	–0.017229
87	$3d^4(^1F)4p\ ^2G^o$	2.327505	2.235385	–0.025760
88	$3d^4(^1F)4p\ ^2D^o$	2.344278	2.254707	–0.023212
89	$3d^4(^3F1)4p\ ^4F^o$	2.362977	2.281233	–0.015384
90	$3d^4(^3P1)4p\ ^4P^o$	2.377718	2.291555	–0.019803
91	$3d^4(^3P1)4p\ ^4D^o$	2.377693	2.292334	–0.018999
92	$3d^4(^3F1)4p\ ^4G^o$	2.401122	2.311476	–0.023285
93	$3d^4(^3P1)4p\ ^2D^o$	2.409313	2.311817	–0.031136
94	$3d^4(^3F1)4p\ ^2F^o$	2.406398	2.314879	–0.025158
95	$3d^4(^3P1)4p\ ^4S^o$	2.435576	2.346541	–0.022676
96	$3d^4(^3F1)4p\ ^2G^o$	2.462172	2.358144	–0.037668
97	$3d^4(^3F1)4p\ ^4D^o$	2.457800	2.359223	–0.032217
98	$3d^4(^3P1)4p\ ^2P^o$	2.467763	2.362016	–0.039387
99	$3d^4(^3P2)4p\ ^2S^o$	2.500439	2.390692	–0.043387
100	$3d^4(^1G1)4p\ ^2H^o$	2.506421	2.399827	–0.040234
101	$3d^4(^1G1)4p\ ^2G^o$	2.504647	2.401050	–0.037237
102	$3d^4(^1G1)4p\ ^2F^o$	2.526987	2.416740	–0.043886
103	$3d^4(^3F1)4p\ ^2D^o$	2.547908	2.426181	–0.055367
104	$3d^4(^1S)4s\ ^2S$	2.441778	–	0.066360
105	$3d^4(^1D1)4p\ ^2P^o$	2.696047	2.560546	–0.069141
106	$3d^4(^1D1)4p\ ^2F^o$	2.747362	2.602964	–0.078038
107	$3d^4(^1D1)4p\ ^2D^o$	2.792989	2.639497	–0.087132
108	$3d^4(^1S)4p\ ^2P^o$	3.015369	–	0.066360

† NIST tables, http://physics.nist.gov/cgi-bin/AtData/main_asd

4. Results

As outlined in our recent work for transitions with the $3d^5$ manifold as an initial check on our work we began our scattering calculations using a similar energy mesh to that used in the work of Zhang & Pradhan (1997). This energy mesh size was insufficient to give converged effective collision strengths. A energy mesh size of 2.5×10^{-5} Rydbergs (≈25 000 energy points) in the resonance region was necessary to resolve all the fine resonance structure. For the transition $3d^5(^2I–^2D3)$ Fig. 2 illustrates the collision strength Ω results as a function of electron energy for the $^1G^o$ scattering symmetry, in the 3 and 7 configuration models. From Fig. 2, in the collision strength one can clearly see the presence of strong resonance features in the vicinity of higher lying thresholds (*X*) and in the near threshold region (*Z*). Furthermore, it is also seen that there is an increase of the background collision strength (*Y*) in the 7 configuration model. All of these features will contribute to an enhancement of the rates at the temperatures considered.

In Figs. 3–6 we illustrate a sample of our effective collision results for transitions between manifolds obtained from the 7 configuration model. Figure 3 is for the transitions $3d^5\ ^6S–3d^4(^5D)4s\ ^4D$ and $3d^5\ ^6S–3d^4(^5D)4s\ ^6D$, Fig. 4 for the transitions $3d^5\ ^6S–3d^4(^5D)4p\ ^6F^o$ and $3d^5\ ^6S–3d^4(^5D)4s\ ^4F^o$. Whereas Fig. 5 is for the transitions $3d^5\ ^4G–3d^4(^5D)4s\ ^4D$ and $3d^5\ ^4G–3d^4(^5D)4s\ ^6D$ and finally Fig. 6 is for the transitions $3d5^4G–3d^4(^5D)4p\ ^6F^o$ and $3d^5\ ^4G–3d^4(^5D)4s\ ^6D^o$.

In Figs. 3 and 4 we include for comparison purposes the Fe IV effective collision results from the calculations of Zhang & Pradhan (1997), averaged over fine-structure levels. From this comparison it is seen that our present effective collision results for non-spin changing forbidden transitions between manifolds give a major enhancement of the rates at all temperatures, whereas for the spin-changing forbidden transitions our present results are comparable to the findings of Zhang & Pradhan (1997). Our recent findings on Fe IV effective collision strengths for transitions within the $3d^5$ manifold, McLaughlin et al. (2005b) with the calculations of Zhang & Pradhan (1997), showed that rates were dramatically increased at temperatures below about 100 000 Kelvin. Therefore given our recent results (McLaughlin et al. 2005b) together with the present findings clearly indicates that the effecive collision strengths data from our calculations should be used in preference to those available in the literature for applications.

Tables 2–17 present all of the non-zero effective collision strengths for the forbidden transitions between the manifolds; i.e., $3d^5–3d^44s$ and $3d^5–3d^44p$, over the temperature range 2000–1 000 000 degrees Kelvin. All of the Fe IV effective collision strength data from Tables 2–17 are available electronically from CDS.

5. Conclusions

We have demonstrated in our previous study and in the current investigation on this ion the importance of including all states arising from a specific manifold in our work. Compared to all previous studies the effects of channel coupling and the importance of including electron correlation effects in our collision

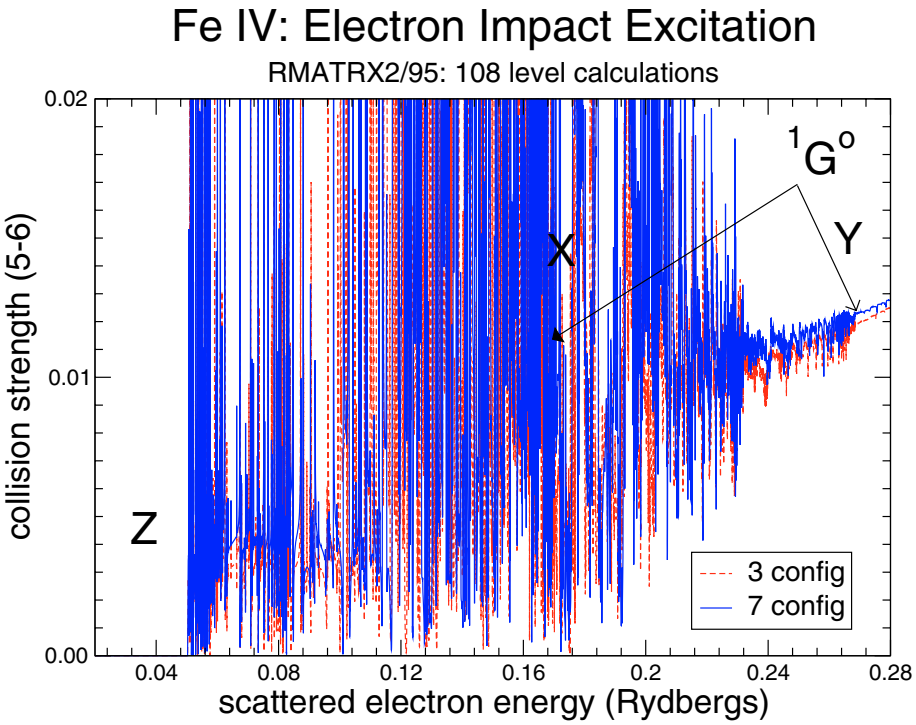

Fig. 2. Fe IV collision strength $\Omega(^2\mathrm{I} - ^2\mathrm{D3})$ for the $^1\mathrm{G^o}$ scattering symmetry as a function of scattering energy. The scattering energy is given in scaled Rydberg units, $\epsilon = E/(z^2 E_{\mathrm{Ryd}})$ where for Fe IV the effective charge $z = N - Z = 3$. The results from the 7 configuration model B, allow for the important core-excitations $3p^2 \rightarrow 3d^2$ in the target and scattering wavefunctions whereas those from the 3 configuration model A do not. Note, model B gives strong resonance enhancement at threshold (Z) and in regions of higher lying thresholds (X). The background collision strength (Y) is also seen to be enhanced.

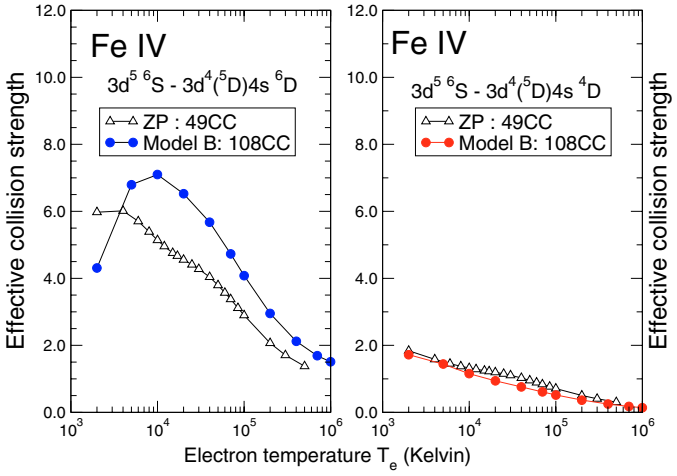

Fig. 3. Fe IV effective collision strength for a sample of transitions between the $3d^5\ ^6S$ ground-state to low-lying states in the $3d^4 4s$ manifolds. The present results were obtained with the 7 configuration model (Model B) which allows for the important core-excitations $3p^2 \rightarrow 3d^2$ in the target and scattering wavefunctions. ZP are the results for the same transitions from the work of Zhang & Pradhan (1997) averaged over fine-structure levels.

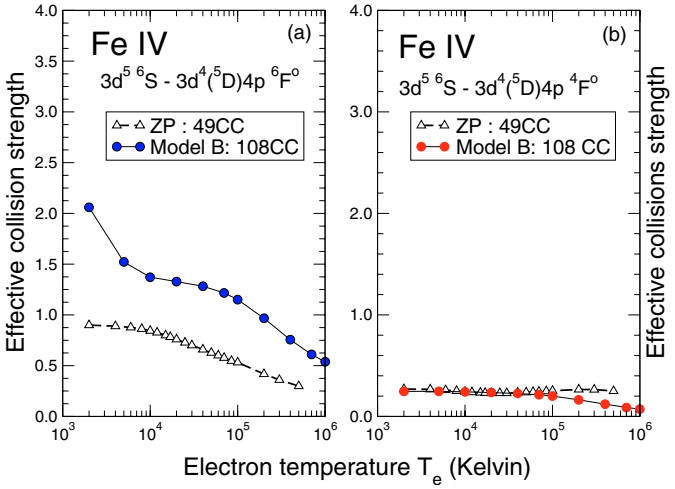

Fig. 4. Fe IV effective collision strength for a sample of transitions between the $3d^5\ ^6S$ ground-state to low-lying states in the $3d^4 4p$ manifolds. The present results were obtained with the 7 configuration model (Model B) which allows for the important core-excitations $3p^2 \rightarrow 3d^2$ in the target and scattering wavefunctions. ZP are the results for the same transitions from the work of Zhang & Pradhan (1997) averaged over fine-structure levels.

model by allowing for the two-electron promotions $3p^2 \rightarrow 3d^2$ in the target wave functions enhance both the collision strength and the rates particularly at low temperatures. The importance of using suitably correlated target and scattering wavefunctions which include core-excitations has been demonstrated in very recent work on the Fe-peak elements, Fe II (Ramsbottom et al. 2004; Ramsbottom et al. 2005), Fe III (McLaughlin et al. 2003, 2005a), Fe IV (McLaughlin et al. 2004, 2005b) and Ni V (Scott et al. 2005). In our work we have used a compact and accurate representation for target and scattering

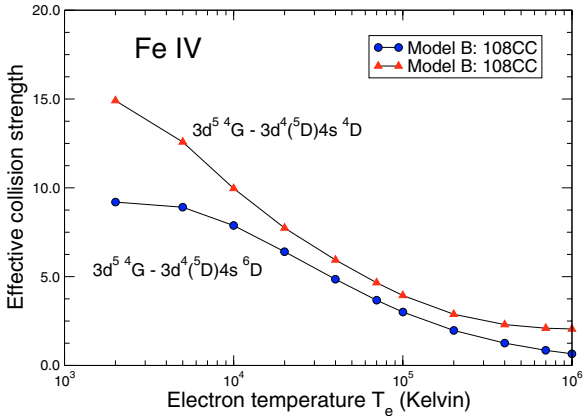

Fig. 5. Fe IV effective collision strength for a sample of transitions between the $3d^5$ ^4G excited state and low-lying states in the $3d^4 4p$ manifolds. The present results were obtained with the 7 configuration model (Model B) which allows for the important core-excitations $3p^2 \rightarrow 3d^2$ in the target and scattering wavefunctions.

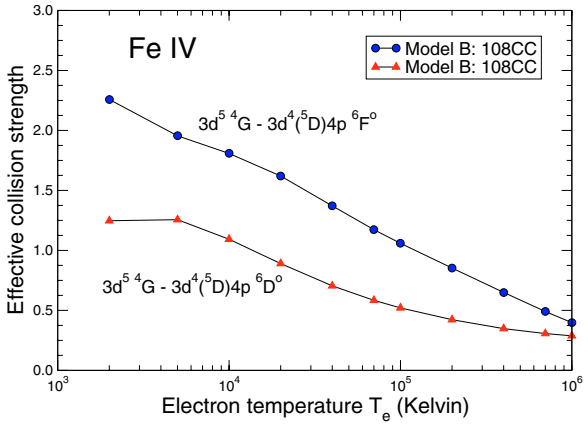

Fig. 6. Fe IV effective collision strength for a sample of transitions between the $3d^5$ ^4G excited state and low-lying states in the $3d^4 4p$ manifolds. The present results were obtained with the 7 configuration model (Model B) which allows for the important core-excitations $3p^2 \rightarrow 3d^2$ in the target and scattering wavefunctions.

wavefunctions. For transitions within the $3d^5$ manifold our recent results on Fe IV for the effective collision strengths (McLaughlin et al. 2005b) compared to previous work showed a major enhancement at low temperatures and ranges from about 20% to almost a factor of two, particularly at low temperatures. For transitions between manifolds our results for the effective collision strengths (for non-spin changing transitions) provide an even greater enhancement, which is consistent with our recent findings on the Fe-peak element Fe III (McLaughlin et al. 2005a). Given the lack of experimental data on this ion to benchmark our calculations, it would appear one can only test the validity of the current results by astronomical observations.

Acknowledgements. Financial support from the UK Particle Physics and Astronomy Research Council (PPARC), under the auspices of a UK Rolling Grant (PPA/G/O/2002/00004) is gratefully acknowledged. The computations were carried out on the HPCX, IBM-Power 4 (SP4), at Daresbury Laboratory, UK, the Cray T3E-1200 and SGI/Origin 2000 CSAR HPC facilities at Manchester University in the UK.

References

Adelman, S. J., Cowley, C. R., Leckrone, D. S., Roby, S. W., & Wahlgren, G. M. 1993, ApJ, 419, 276
Becker, S. R., & Butler, K. 1995, A&A, 301, 187
Berrington, K. A., & Pelan, J. C. 1995a, ApJS, 114, 367
Berrington, K. A., & Pelan, J. C. 1995b, ApJS, 119, 189
Burke, P. G., & Robb, W. D. 1975, Adv. At. Mol. Phys., 11, 143
Burke, P. G., Hibbert, A., McLaughlin, B. M., et al. 2004, Contributed papers of the Gaseous Electronics Conference, Bunratty Castle, Ireland: Bull. Am. Phys. Soc., 49, 25
Clementi, E., & Roetti, C. 1974, At. Data & Nucl. Data Tables, 14, 177
Esteban, C., Piembert, M., Garcia-Rojas, J., et al. 2004, MNRAS, 355, 229
Eissner, W., Martins, P., De, A. P., Nussbaumer, H., Saraph, H. E., & M. J., Seaton 1969, MNRAS, 146, 63
Hibbert, A. 1975, Comput. Phys. Commun., 9, 141
Hibbert, A., Correge, G., McLaughlin, B. M., Ramsbottom, C. A., & Scott, M. P. 2004, Bull. Am. Phys. Soc., 49, 75
Holberg, J. B., Hubeny, I., Barstow, M. A., et al. 1994, ApJ, 425, L105
McKenna, F. C., Keenan, F. P., Hambly, N. C., Allende Prieto, C., & Rolleston, W. R. J. 1997, ApJ, 109, 225
McLaughlin, B. M., Scott, M. P., Sunderland, A. G., et al. 2003, Contributed papers of the ICPEAC XX, Stockholm, Sweden Th088
McLaughlin, B. M., Hibbert, A., Scott, M. P., et al. 2004, Bull. Am. Phys. Soc., 49, 69
McLaughlin, B. M., Scott, M. P., Sunderland, A. G., et al. 2005a, At. Data & Nucl. Data Tables, submitted
McLaughlin, B. M., Hibbert, A., Scott, M. P., et al. 2005b, J. Phys. B: At. Mol. Opt. Phys., 38, 2029
Noble, C. J. 2004, Phys. Scr., T110, 233
Noble, C. J., Burke, V. M., & Burke, P. G. 2005, Comput. Phys. Commun., in preparation
Penston, M. V., Benvenuti, P., Cassatella, A., et al. 1983, MNRAS, 202, 883
Quinet, P., & Hansen, J. E. 1995, J. Phys. B: At. Mol. Opt. Phys., 28, L213
Ramsbottom, C. A., Noble, C. J., Burke, V. M., Scott, M. P., & Burke, P. G. 2004, J. Phys. B: At. Mol. Opt. Phys., 37, 3609
Ramsbottom, C. A., Noble, C. J., Burke, V. M., et al. 2005, J. Phys. B: At. Mol. Opt. Phys., 38, 2999
Rubin, R. H., Dufour, R. J., Ferland, G. J., et al. 1997, ApJ, 474, L131
Ruiz-Lapuente, P., Kirshner, R. P., Phillips, M. M., et al. 1995, ApJ, 439, 60
Sawey, P. M. J., & Berrington, K. A. 1992, J. Phys. B: At. Mol. Opt. Phys., 25, 1451
Scott, M. P., Ramsbottom, C. A., Noble, C. J., Burke, V. M., & Burke, P. G. 2005, J. Phys. B: At. Mol. Opt. Phys., submitted
Sugar, J., & Corliss, J. 1985, J. Phys. Chem. Ref. Data Suppl., 2, 14
Sunderland, A. G., Burke, P. G., Burke, V. M., & Noble, C. J. 1999, in High Performance Computing, ed. R. J. Allan, M. F. Guest, A. D. Simpson, D. S. Henty, & D. A. Nicole (New York & London: Kluwver Academic), 293
Sunderland, A. G., Burke, V. M., Noble, C. J., & Burke, P. G. 2002, Comput. Phys. Commun., 145, 311
Zhang, H. L., & Pradhan, A. K. 1997, A&AS, 126, 373